Laser emission of a Nd-doped mixed tellurite and zinc oxide glass

M. J. V. Bell,[1,*] V. Anjos,[1] L. M. Moreira,[1] R. F. Falci,[1] L. R. P. Kassab,[2] D. S. da Silva,[3] J. L. Doualan,[4] P. Camy,[4] and R. Moncorgé[4]

[1]*Laboratório de Espectroscopia de Materiais, Departamento de Física, Universidade Federal de Juiz de Fora, Juiz de Fora-MG, Brazil*

[2]*Laboratório de Tecnologia em Materiais Fotônicos e Optoeletrônicos, Faculdade de Tecnologia de São Paulo, CEETEPS/UNESP, Saõ Paulo, Brazil*

[3]*Departamento de Engenharia de Sistemas Eletrônicos, Escola Politécnica da USP, São Paulo, Brazil*

[4]*Centre de Recherche sur les Ions, les Matériaux et la Photonique (CIMAP), UMR CNRS-CEA-Ensicaen, Universite de Caen, 6 Boulevard Maréchal Juin, F-14050 Caen, France*

**Corresponding author: mjbell@fisica.ufjf.br*

Received March 21, 2014; revised April 28, 2014; accepted April 29, 2014; posted May 12, 2014 (Doc. ID 208332); published June 19, 2014

The present work reports the luminescence properties and the laser operation of a Nd^{3+}-doped (TeO_2-ZnO) bulk tellurite glass. The spectroscopic data are analyzed within the framework of the Judd–Ofelt formalism and the results are used in conjunction with fluorescence lifetime and emission measurements to derive values for the quantum efficiency and the stimulated emission cross section of the considered $^4F_{3/2} \rightarrow {}^4I_{11/2}$ infrared laser transition around 1062.5 μm. Continuous-wave laser action is achieved for the first time with this bulk tellurite glass by pumping the sample inside a standard two-mirror laser cavity with different output couplers. A low-threshold pump power of 8 mW associated with a laser slope efficiency of 21% could be obtained for an output coupler transmission of 2.7%.

OCIS codes: (140.3530) Lasers, neodymium; (140.5680) Rare earth and transition metal solid-state lasers; (170.6280) Spectroscopy, fluorescence and luminescence; (300.6500) Spectroscopy, time-resolved.

http://dx.doi.org/10.1364/JOSAB.31.001590

1. INTRODUCTION

Although interest for Yb^{3+}-doped laser materials for short-pulse and high-peak power laser systems is continuously increasing, the Nd^{3+}-doped laser materials still remain very attractive and extensively studied for a wide variety of applications because of their much easier 4-level laser operation mode and usually higher gain cross sections [1]. Namely, although laser action of Nd^{3+} has been demonstrated in a large number of crystals and glasses, the search for Nd^{3+}-doped new solid-state laser hosts having specific thermo-mechanical and optical properties is still very active. This is the case for the instance of the recently developed CaF_2 laser crystal codoped with Nd^{3+} and Lu^{3+} or Y^{3+} ions, because of the conjunction of good thermo-mechanical properties, typical of crystals, and broadband spectral properties, typical of glasses [2]. This is also the case for some Nd-doped nonlinear tellurite glasses [3–9], because of a very interesting combination of large nonlinear refractive index (25 times larger than that of silica) and wide transmittance range, and also because of a low maximum phonon frequency which allows rare-earth ion laser emissions in a wide spectral range [10].

More generally, crystalline laser hosts lead to higher absorption and emission cross section, while glasses can be produced in larger volumes with optimal optical quality. In order to minimize the nonradiative multiphonon relaxations and optimize the quantum efficiency of the $^4F_{3/2} \rightarrow {}^4I_{11/2}$ emission of Nd^{3+}, it is also suitable to work with Nd^{3+}-doped host materials with low phonon frequencies and low contents of OH impurities. In that sense, laser emission of Nd^{3+} in glasses has been reported in fluorides [11–13], chalcogenides [14], aluminosilicates [15], germanates [16], and, as just mentioned, in tellurite glasses [3–7]. Among oxi-tellurites, the TeO_2-ZnO glass which is considered here in the present article combines good mechanical stability, chemical durability, high linear and nonlinear refractive indices, together with low phonon energies (~750 cm^{-1}), a wide transmission window (0.4–6 μm), and a high rare-earth solubility [10,17,18]. The large linear refractive indices ($1.8 < n < 2.3$) [10,17] of tellurite glasses imply large stimulated emission cross sections, sometimes larger than for phosphate glasses [19]. Their high nonlinear optical properties can be used advantageously for the development of Kerr-lens mode-locked subpicosecond lasers. Spectroscopic [20,21] and thermo-optical properties [22,23] of these tellurite glasses have been also studied in recent years for the possibility of using thin films for the fabrication of rib waveguides [24] and for the possibility of increasing the luminescent quantum yield of rare-earth ions, in general, by codoping the materials with silver nanoparticles [20,21].

The present work concentrates on the luminescence properties and the laser performance of a TeO_2-ZnO- (TZO) mixed tellurite and zinc oxide glass doped with Nd^{3+}. True continuous-wave (CW) laser action is achieved by pumping the sample with a CW Ti:sapphire laser inside a standard two-mirror laser cavity. A low laser threshold of 8 mW and

a laser slope efficiency of 21% could be obtained for an output coupler transmission of 2.7%, which is an encouraging improvement compared to what was reported in the past with other Nd-doped tellurite bulk glasses [3–7].

2. EXPERIMENTAL DETAILS

The investigated spectroscopic and laser samples were prepared by using the melting–quenching technique with the following composition (in wt%): 85%TeO_2-15%ZnO (TZO). It was doped with 1.0%Nd_2O_3. Reagents were melted at 800°C in an platinum crucible for 20 min, quenched in a preheated brass mold, annealed at 325°C for 2 h, and cooled down to room temperature during 2 h to avoid internal stresses.

The absorption spectra were registered both between about 300 and 1000 nm, by using a Shimadzu model 2445 UV–VIS–NIR monochromator, and between about 2000 and 7000 cm^{-1}, with a FT–IR spectrophotometer. The emission spectra and the fluorescence lifetime measurements were achieved by exciting the sample with a diode laser emitting at 808 nm (100 mW) and chopped at 100 Hz. The luminescence signal was collected and dispersed through a Tzerny–Turner monochromator (Spectral Products model TK488). It was detected by a 928 PMT detector and analyzed by a SRS 555 lock-in amplifier or a TDS2020 oscilloscope coupled to a computer for the spectral or the lifetime data.

The laser setup consisted in a standard plano-concave laser resonator. The flat dichroic mirror was highly reflective ($R > 99.5\%$) around 1064 nm and highly transmittive ($T > 95\%$) around 808 nm. Three different concave output mirrors with a radius of curvature of 100 mm and transmissions of 0.8%, 2.7%, and 8% around 1064 nm were used. The laser sample was prepared in the form of a 10 mm × 10 mm platelet of 2 mm thickness, with carefully polished and parallel end-faces but without any antireflection coatings. It was fixed with silver paste on a copper sample holder without any particular cooling and pumped through the dichroic input mirror by using a CW Ti: sapphire laser tuned at 806 nm and focused with a lens of 10 cm focal length.

3. SPECTROSCOPIC AND LUMINESCENCE PROPERTIES

The UV-VIS-NIR absorbance (optical density) spectrum of the sample, as registered between 350 and 950 nm, is shown in Fig. 1(a). The features corresponding to the main absorption transitions of Nd^{3+} from its $^4I_{9/2}$ fundamental level to its $^4F_{3/2}$ (890 nm), $^4F_{5/2} + {}^2H_{9/2}$ (808 nm), $^4F_{7/2} + {}^4S_{3/2}$ (750 nm), $^4F_{9/2}$ (690 nm), $^4G_{5/2} + {}^2G_{7/2}$ (580 nm), and $^4G_{7/2} + {}^4G_{9/2} + {}^2K_{13/2}$ excited manifolds have been identified and reported in the figure. As expected for glass, the absorption features appear as broad bands, which is favorable for diode pumping. Figure 1(b) shows the FT-IR transmission spectrum between about 2000 and 7000 cm^{-1}. It indicates the presence in the glass of a very low but non-negligible amount of OH radicals.

The UV-VIS-NIR absorption spectrum was then analyzed within the framework of the Judd–Ofelt (JO) formalism [25,26]. This led to the following JO parameters: $\Omega_2 = 3.09 \times 10^{-20}$ cm^2, $\Omega_4 = 3.11 \times 10^{-20}$ cm^2, and $\Omega_6 = 3.25 \times 10^{-20}$ cm^2, with a RMS $= 0.1 \times 10^{-20}$ cm^2. This analysis also allowed us to derive a radiative rate for the $^4F_{3/2} \rightarrow {}^4I_{11/2}$ emission transition $A(^4F_{3/2} \rightarrow {}^4I_{11/2}) \approx 2182$ s^{-1}, a total

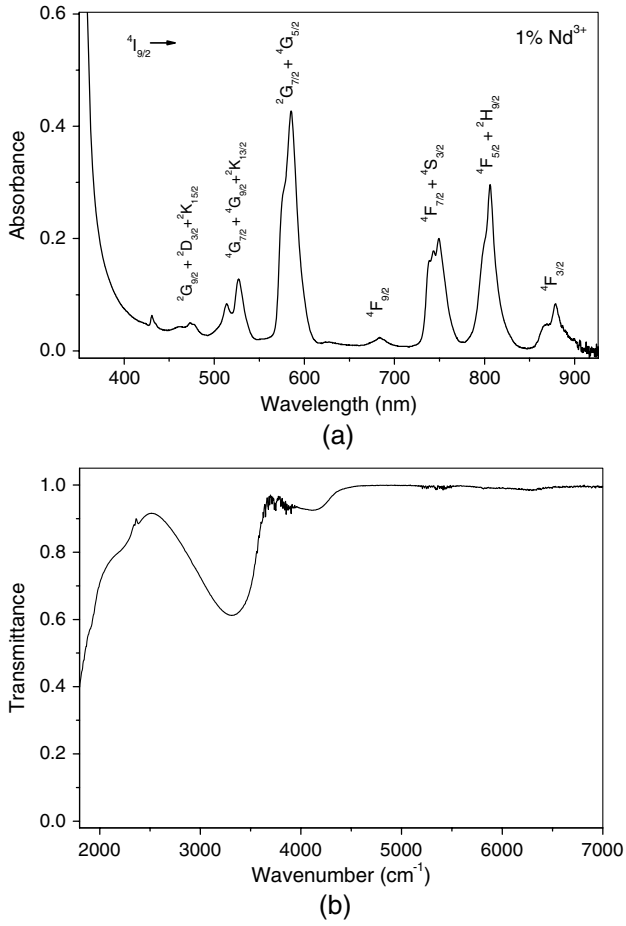

Fig. 1. (a) UV-VIS-NIR absorbance and (b) FTIR transmittance spectra for a sample doped with 1%Nd (1.9×10^{19} ions/cm^3) and 1.64 mm thickness.

radiative emission lifetime for the $^4F_{3/2}$ laser emitting level $\tau_R = 217.5$ μs, and branching ratios $\beta_{9/2} = 42.8\%$, $\beta_{11/2} = 47.4\%$, $\beta_{13/2} = 9.32\%$, and $\beta_{15/2} = 0.48\%$ for the $^4F_{3/2} \rightarrow {}^4I_{9/2}$, $^4I_{11/2}$, $^4I_{13/2}$, and $^4I_{15/2}$ emission transitions (see Fig. 2) occurring around 900, 1060, 1350, and (not observed) 1800 nm, respectively.

Figure 2 exhibits the near-infrared luminescence spectrum of the sample obtained after excitation at 806 nm within the

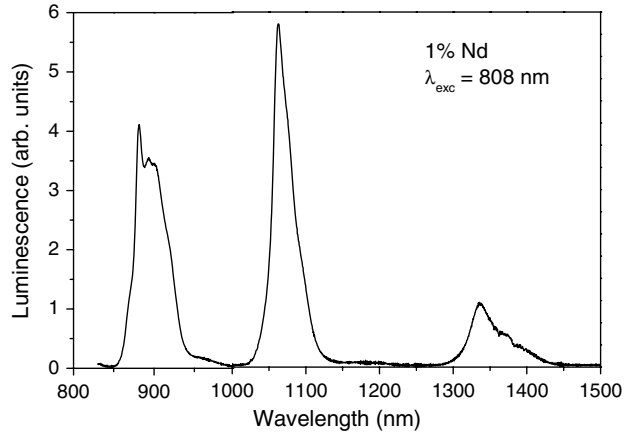

Fig. 2. Near-infrared luminescence of the TZO glass doped with 1% Nd_2O_3 (wt).

$^4I_{9/2} \rightarrow {}^4F_{5/2} + {}^2H_{9/2}$ absorption band [see Fig. 1(a)]. It consists of three broadband emissions peaking around 882, 1062, and 1335.5 nm. They are assigned to the three usual Nd^{3+} emission transitions, $^4F_{3/2} \rightarrow {}^4I_{9/2}$, $^4F_{3/2} \rightarrow {}^4I_{11/2}$, and $^4F_{3/2} \rightarrow {}^4I_{13/2}$, and they are associated with the experimental branching ratios (fraction of photons emitted within each of the emission transitions) $\beta_{9/2} = 44\%$, $\beta_{11/2} = 41\%$, and $\beta_{13/2} = 15\%$, with $\beta_i = (\int_i \lambda I_i(\lambda)\mathrm{d}\lambda / \sum_{i=1,2,3} \int_i \lambda I_i(\lambda)\mathrm{d}\lambda)$ and $i = 9/2$, 11/2, and 15/2, respectively. The result obtained for $\beta_{9/2}$ is very close to that found from the absorption spectrum and the JO treatment. The values found for the other two transitions are different but remain close to the previous ones within the experimental uncertainties. In view of the very good RMS value obtained with the JO treatment, and the more delicate procedure to get perfectly calibrated emission spectra (the problem of correction from the spectral response of the equipment and the problem of reabsorption which always affects the shape and the intensity of the emission transition around 900 nm), a better fit will be given in the following for the values derived with the JO analysis. It is also worth noting here that no visible upconversion emission was observed "by eye" with the considered excitation conditions.

Figure 3 shows the fluorescence decay associated with the $^4F_{3/2} \rightarrow {}^4I_{11/2}$ emission transition around 1063 nm. The decay is fully exponential with a fluorescence time constant $\tau_f = 209$ μs. Therefore, according to the above calculated radiative lifetime $\tau_R = 217$ μs, the quantum efficiency for the $^4F_{3/2} \rightarrow {}^4I_{11/2}$ emission transition, i.e., $\eta = \tau_f/\tau_R$, is found equal to about 96%. It also means that no concentration quenching occurs in this material at the considered 1%Nd dopant concentration, which is not the case, for instance, with the Nd-doped tellurite glass investigated in [3].

Based on the above derived spectroscopic and luminescence data, the emission spectrum reported in Fig. 2 can be further exploited to estimate the stimulated emission cross section of the considered $^4F_{3/2} \rightarrow {}^4I_{11/2}$ emission transition peaking around 1062.5 nm by using the usual expression [27]

$$\sigma_{\mathrm{em}}(\lambda) = \frac{\lambda^4}{8\pi c n^2 \Delta\lambda} \cdot A(^4F_{3/2} \rightarrow {}^4I_{9/2}), \tag{1}$$

where $\Delta\lambda$ stands for the width of the emission line at half-maximum and $n \approx 2$ is the refractive index of the material [28].

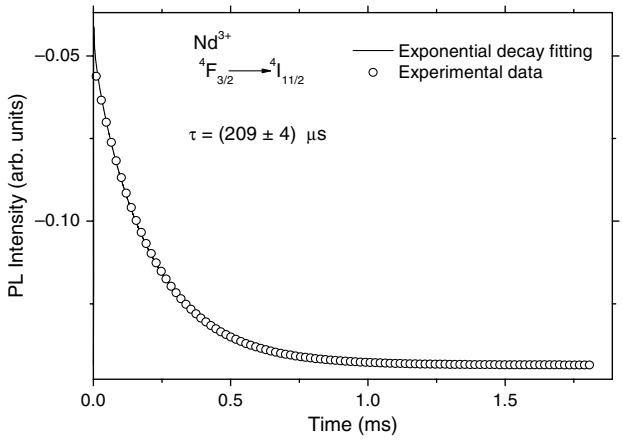

Fig. 3. Luminescence decay of the TZO glass doped with 1% Nd_2O_3 (wt).

This expression leads to the emission cross section $\sigma_{\mathrm{em}}(1062.5\ \mathrm{nm}) \approx 3.14 \times 10^{-20}\ \mathrm{cm}^2$.

4. CW LASER RESULTS

Figure 4 shows the laser output versus absorbed pump power curves obtained after pumping the sample around 806 nm. Threshold pump powers of 17, 8, and 85 mW (or 17, 24, and 100 mW, as extrapolated with the straight lines reported in the figure) and slope efficiencies of 16%, 21%, and 14.5% were obtained for the output coupler transmissions of 0.8%, 2.7%, and 8%, respectively.

These curves can be exploited to estimate the intrinsic round trip optical losses noted as L inside the laser cavity, thus to have an idea of the optical quality of the laser sample. For that purpose, use can be made of the Findlay–Clay or the Caird technique [29,30]. The first one consists of a plot of the threshold pump power P_{th} versus the transmission T of the output coupler and the second one in a plot of the inverse of the slope efficiency η^{-1} versus the inverse of the transmission T^{-1}. Knowing the expressions

$$P_{\mathrm{th}} = aT + b, \tag{2}$$

and

$$\eta^{-1} = a'T^{-1} + b', \tag{3}$$

with [31]

$$a = \frac{h\upsilon_L S}{2\eta_q \sigma_{\mathrm{em}} \eta_e \tau_R \eta_R \varepsilon_p \eta_p}, \qquad b = aL,$$

$$a' = b'L, \quad \text{and} \quad b' = \frac{1}{\eta_q \eta_e \varepsilon_p \eta_p},$$

where υ_L stands for the laser emission frequency, $S \approx \pi(\varpi_p^2 + \varpi_c^2)/2$ with ϖ_p and ϖ_c the pump and cavity mode waist radii, respectively, σ_{em} the stimulated emission cross section, $\eta_q = (\lambda_p/\lambda_L)$ the quantum conversion efficiency, $\eta_e = (\sigma_{\mathrm{em}}^{\mathrm{eff}}/\sigma_{\mathrm{em}})$ with $\sigma_{\mathrm{em}}^{\mathrm{eff}} = (\sigma_{\mathrm{em}} + \sigma_a - \sigma_{\mathrm{esa}})$, $\eta_R = (\tau_f/\tau_R)$ the radiative quantum efficiency, ε_p the pump efficiency, i.e., the fraction of absorbed pump photons in the laser levels, and $\eta_p = 1 - \exp(-\sigma_p N l)$ the fraction of absorbed versus

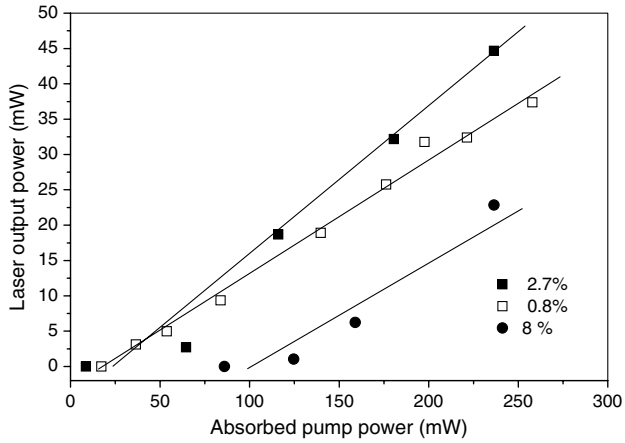

Fig. 4. Laser output versus absorbed pump power curves obtained after pumping the TZO glass sample around 806 nm, for the output coupler transmissions of 0.8%, 2.7%, and 8%.

Table 1. Laser Cavity Parameters of Several Nd^{3+} Tellurite Glasses Reported in the Literature[a]

	Tellurite Glasses				
Parameter	Lei *et al.* [7]	Kalaycioglu *et al.* [5]	Miguel *et al.* [4]	Michel *et al.* [3]	This Work
Glass structure	86.6%TeO_2-8.4%BaO-4.0%NaO-1%ZnO (wt)	0.8%TeO_2-0.2%WO_3 (mole)	74.6%TeO_2-8.8%ZnO-16.6%ZnF_2 (mole)	95.5%TeO_2-4.5%Li_2O (wt)	85.0%TeO_2-15.0%ZnO (wt)
λ_{laser} (nm)	1066	1065	1059	1065	1062
λ_{pump} (nm)	804.3	805	802	514.5	806
η_{slope}	14.7%	12%	—	14%	21%
P_{th}	4.2 mJ	11 μJ	27 mJ	20 mW	8 mW
T	4%	3.3%	HR	1%	2.7%
%Nd	1%Nd_2O_3	0.5%Nd_2O_3	1%NdF_3	5%Nd_2O_3	1%Nd_2O_3
τ_f, τ_R (μs)	170, -	142, 149	128, 145	56, 199	209, 217
$\Delta\lambda$ (nm)	15	29	22	5.4	29.3
σ_{em} (cm^2)	3.9×10^{-20}	3.2×10^{-20}	4.9×10^{-20}	4.7×10^{-20}	3.1×10^{-20}

[a] λ_{laser}, λ_{pump}, η_{slope}, T, L, P_{th}, and σ_{emiss} means emission wavelength, pumping wavelength, slope efficiency, output coupled transmission, threshold, and stimulated emission cross section, respectively.

incident pump photons. Without entering into the details of the values of all these parameters, the first type of plot, when use is made of the threshold pump powers extrapolated with the straight lines of Fig. 4, leads to round trip optical losses $L \approx 0.3\%$. Alternatively, by using the second type of plot and the values for the laser slope efficiencies obtained with the output coupler transmissions of 0.8% and 2.7% essentially, the one obtained for the output coupler transmission of 8% being too approximative, it is found to have round trip optical losses $L \approx 0.4\%$. Therefore, it can be safely concluded that the laser material introduces single-pass optical losses less than 0.2%, which is quite good.

Finally, Table 1 gives a comparison between these laser results and those obtained in the past for different tellurite glasses. It shows that the investigated Nd-doped TeO_2-ZnO glass gives rise to a significant improvement in the laser slope efficiency.

5. CONCLUSIONS

We have demonstrated true CW laser action in a bulk Nd^{3+}-doped TeO_2-ZnO tellurite glass at 1062 nm, with a low laser threshold of 8 mW and a slope efficiency of 21% for an output mirror transmission of only 2.7%. Such a laser result still remains modest (likely because of non-AR-coated sample faces and nonoptimized pump and laser cavity modes) but it is more significant than the results reported in the past with other Nd-doped tellurite bulk glasses. The obtained efficiency is exceeded only by a 60 cm long Nd-doped tellurite glass fiber (76.9%TeO_2-6.0%Na_2O 15.5%ZnO-1.5%Bi_2O_3-0.1%Nd_2O_3) for which it was reported a laser slope efficiency of 46% for a lasing threshold of 27 mW [32]. This result proves that the achieved optical quality (attested by low internal losses) is improved compared to the previously studied bulk tellurite systems. This is also due to a fairly long emission lifetime of about 210 μs, an emission quantum efficiency nearly equal to 1 and a reasonably large stimulated emission cross section of 3.1×10^{-20} cm^2 for a fairly wide emission bandwidth of 29 nm. Such characteristics, along with its inherent nonlinear optical properties, suggest that the present tellurite laser glass opens the way to further developments both in the form of bulk and waveguide photonic devices for various types of applications, including the generation of ultrashort mode-locked laser pulses.

ACKNOWLEDGMENTS

The authors acknowledge the financial support of the Brazilian agencies CAPES, FAPEMIG National Institute of Photonics (INCT Project/CNPq), CAPES/COFECUB, and CNPq.

REFERENCES

1. F. Träger, ed., *Handbook of Lasers and Optics* (Springer, 2007), pp. 636–648.
2. J. L. Doualan, L. B. Su, G. Brasse, A. Benayad, V. Ménard, Y. Y. Zhan, A. Braud, P. Camy, J. Xu, and R. Moncorgé, "Improvement of infrared laser properties of Nd:CaF_2 crystals via codoping with Y^{3+} and Lu^{3+} buffer ions," J. Opt. Soc. Am. B **30**, 3018–3021 (2013).
3. J. C. Michel, D. Morin, and F. Auzel, "Propriétés spectroscopiques et effet laser d'un verre tellurite et d'un verre phosphate dopés en néodyme," Rev. Phys. Appl. **13**, 859–866 (1978).
4. A. Miguel, J. Azkargorta, R. Morea, I. Iparraguirre, J. Gonzalo, J. Fermamdez, and R. Balda, "Spectral study of the stimulated emission of Nd^{3+} in fluorotellurite bulk glass," Opt. Express **21**, 9298–9307 (2013).
5. H. Kalaycioglu, H. Cankaya, G. Ozen, L. Ovecoglu, and A. Sennaroglu, "Lasing at 1065 nm in bulk Nd^{3+}-doped telluride–tungstate glass," Opt. Commun. **281**, 6056–6060 (2008).
6. I. Iparraguirre, J. Azkargorta, J. M. Fernández-Navarro, M. Al-Saleh, J. Fernández, and R. Balda, "Laser action and upconversion of Nd^{3+} in tellurite bulk glass," J. Non-Cryst. Solids **353**, 990–992 (2007).
7. N. Lei, B. Xu, and Z. H. Jiang, "Ti–sapphire laser pumped Nd–tellurite glass laser," Opt. Commun. **127**, 263–265 (1996).
8. W. Ryba-Romanowski, S. Golab, L. Cichosz, and B. J. Ttzebiatowska, "Influence of temperature and acceptor concentration on energy transfer from Nd^{3+} to Yb^{3+} and from Yb^{3+} to Er^{3+} in tellurite glass," J. Non-Cryst. Solids **105**, 295–302 (1988).
9. J. S. Wang, E. M. Vogel, E. Snitzer, J. L. Jackel, V. L. da Silva, and Y. Silberberg, "1.3 μm emission of neodymium and praseodymium in tellurite-based glasses," J. Non-Cryst. Solids **178**, 109–113 (1994).
10. R. A. H. El-Mallawany, *Tellurite Glasses Handbook: Physical Properties and Data* (CRC Press, 2001).
11. R. R. Petrin, M. L. Kliewer, J. T. Beasley, R. C. Powell, I. D. Aggarwal, and R. C. Ginther, "Spectroscopy and laser operation of Nd:ZBAN glass," IEEE J. Quantum Electron. **27**, 1031–1038 (1991).
12. J. Azkargorta, I. Iparraguirre, R. Balda, J. Fernández, E. Dénoue, and J. L. Adam, "Spectroscopic and laser properties of Nd3+ in

BIGaZLuTMn fluoride glass," IEEE J. Quantum Electron. **30**, 1862–1867 (1994).
13. J. Azkargorta, I. Iparraguirre, R. Balda, and J. Fernández, "On the origin of bichromatic laser emission in Nd^{3+}-doped fluoride glasses," Opt. Express **16**, 11894–11906 (2008).
14. T. Schweizer, D. W. Hewak, D. N. Payne, T. Jensen, and G. Huber, "Rare-earth doped chalcogenide glass laser," Electron. Lett. **32**, 666–667 (1996).
15. D. F. de Sousa, L. A. O. Nunes, J. H. Rohling, and M. L. Baesso, "Laser emission at 1077 nm in Nd^{3+}-doped calcium aluminosilicate glass," Appl. Phys. B **77**, 59–63 (2003).
16. J. Fernandez, I. Iparraguirre, R. Balda, J. Azkargorta, M. Voda, and J. M. Fernandez-Navarro, "Laser action and upconversion of Nd^{3+} in lead–niobium–germanate bulk glass," Opt. Mater. **25**, 185–191 (2004).
17. J. S. Wang, E. M. Vogel, and E. Snitzer, "Tellurite glass: a new candidate for fiber devices," Opt. Mater. **3**, 187–203 (1994).
18. A. Jha, S. Shen, and M. Naftaly, "Structural origin of spectral broadening of 1.5-μm emission in Er3+ doped tellurite glasses," Phys. Rev. B **62**, 6215–6227 (2000).
19. M. J. Weber, "Science and technology of laser glass," J. Non-Cryst. Solids **123**, 208–222 (1990).
20. L. R. P. Kassab, L. F. Freitas, T. A. A. de Assumpção, D. M. da Silva, and C. B. de Araújo, "Frequency upconversion properties of Ag: TeO2–ZnO nanocomposites codoped with Yb^{3+} and Tm^{3+} ions," Appl. Phys. B **104**, 1029–1034 (2011).
21. T. A. A. de Assumpção, M. E. Camilo, L. R. P. Kassab, A. S. L. Gomes, C. B. de Araújo, and N. U. Wetter, "Frequency upconversion properties of Tm^{3+} doped TeO2–ZnO glasses containing silver nanoparticles," J. Alloys Compd. **536**, S504–S506 (2012).
22. L. R. P. Kassab, R. A. Kobayashi, M. J. V. Bell, A. P. Carmo, and T. Catunda, "Thermo-optical parameters of tellurite glasses doped with Yb^{3+}," J. Phys. D Appl. Phys. **40**, 4073–4077 (2007).
23. A. P. Silva, A. P. Carmo, V. Anjos, M. J. V. Bell, L. R. P. Kassab, and R. A. Pinto, "Temperature coefficient of optical path of tellurite glasses doped with gold nanoparticles," Opt. Mater. **34**, 239–243 (2011).
24. V. D. Del Cacho, A. L. Siarkowsi, N. Morimoto, H. V. Borges, and L. R. P. Kassab, "Fabrication and characterization of TeO_2–ZnO rib waveguides," ECS Transactions **31**, 225–229 (2010).
25. B. R. Judd, "Optical absorption intensities of rare-earth ions," Phys. Rev. **127**, 750–761 (1962).
26. G. S. Ofelt, "Intensities of crystal spectra of rare-earth ions," J. Chem. Phys. **37**, 511–520 (1962).
27. W. K. Krupke, "Induced emission cross-sections in neodymium laser glasses," IEEE J. Quantum Electron. **10**, 450–457 (1974).
28. A. A. Sidek, S. Rosmawati, Z. A. Talib, M. K. Halimah, and W. M. Daud, "Synthesis and optical properties of ZnO–TeO2 glass system," Am. J. Appl. Sci. **6**, 1489–1494 (2009).
29. D. Findlay and R. A. Clay, "The measurement of internal losses in 4-levels lasers," Phys. Lett. **20**, 277–278 (1966).
30. J. A. Caird, S. A. Payne, P. R. Staver, A. J. Ramponi, L. L. Chase, and W. F. Krupke, "Quantum electronic properties of $Na_3Ga_2Li_3F_{12}:Cr^{3+}$," J. Quantum Electron. **24**, 1077–1099 (1988).
31. R. Moncorgé, "Current topics in rare-earth lasers," in *Spectroscopic Properties of Rare-Earths in Optical Materials*, G. Liu and B. Jacquier, eds., Springer Series in Materials Science (Springer, 2005), Chap. 6, pp. 320–378.
32. J. S. Wang, D. P. Machewi, F. Wu, E. Snitzer, and E. M. Vogel, "Neodymium-doped tellurite single-mode fiber laser," Opt. Lett. **19**, 1448–1449 (1994).